

## ANALYTIC CROSS SECTIONS FOR SUBSTRUCTURE LENSING

CHARLES R. KEETON<sup>1</sup>

Astronomy and Astrophysics Department, University of Chicago,  
5640 S. Ellis Ave., Chicago, IL 60637  
*To appear in The Astrophysical Journal*

### ABSTRACT

The magnifications of the images in a strong gravitational lens system are sensitive to small mass clumps in the lens potential; this effect has been used to infer the amount of substructure in galaxy dark matter halos. I study the theory of substructure lensing to identify important general features, and to compute analytic cross sections that will facilitate further theoretical studies. I show that the problem of a clump anywhere along the line of sight to a lens can be mapped onto an equivalent problem of a clump in a simple convergence and shear field; clumps at arbitrary redshifts are therefore not hard to handle in calculations. For clumps modeled as singular isothermal spheres (SIS), I derive simple analytic estimates of the cross section for magnification perturbations of a given strength. The results yield two interesting conceptual points. First, lensed images with positive parity are always made brighter by SIS clumps; images with negative parity can be brightened but are much more likely to be dimmed. Second, the clumps need not lie within the lens galaxy; they can be moved in redshift by several tenths and still have a significant lensing effect. Isolated small halos are expected to be common in hierarchical structure formation models, but it is not yet known whether they are abundant enough compared with clumps inside lens galaxies to affect the interpretation of substructure lensing.

*Subject headings:* gravitational lensing — cosmology: theory — dark matter — large-scale structure of universe

### 1. INTRODUCTION

Strong gravitational lensing directly probes the mass distributions of cosmological objects. In quadruply-imaged quasars and radio sources, the flux ratios between the images provide a powerful test of the smoothness of galaxy mass distributions at redshifts  $z \sim 0.2$ – $1$ . The popular Cold Dark Matter (CDM) paradigm predicts that galaxy dark matter halos are not smooth but rather full of small mass clumps (e.g., Klypin et al. 1999; Moore et al. 1999), which can perturb lens flux ratios in ways that cannot be explained by smooth lens models (e.g., Mao & Schneider 1998; Metcalf & Madau 2001; Bradač et al. 2002; Chiba 2002; Metcalf & Zhao 2002).

This “substructure lensing” effect has been detected both individually (Mao & Schneider 1998; Keeton 2001b; Bradač et al. 2002) and statistically (Dalal & Kochanek 2002a). The statistical detection implies that  $f_{\text{clump}} \sim 2\%$  (0.6–7% at 90% confidence) of galaxies’ mass is in small clumps, and this result has been used to constrain the power spectrum on small scales (Dalal & Kochanek 2002b). It suggests that the “missing satellite” problem in CDM (e.g., Klypin et al. 1999; Moore et al. 1999) is solved not by warm or exotic dark matter (e.g., Spergel & Steinhardt 2000; Colin, Avila-Reese & Valenzuela 2000; Bode, Ostriker & Turok 2001) but rather by astrophysical mechanisms that suppress star formation in small clumps (e.g., Bullock, Kravtsov & Weinberg 2000; Somerville 2002; Benson et al. 2002). In other words, Dalal & Kochanek (2002a) argue, real galaxies contain numerous mass clumps that are predominantly dark.

The theory of substructure lensing is still young. To date, studies have relied mainly on Monte Carlo simulations and have explored relatively small parameter spaces. To estimate the magnitude of the effect and demonstrate

its measurability. Chiba (2002) fixed the clump population based on results from  $N$ -body simulations, while Metcalf & Madau (2001) adopted a clump mass function from simulations and varied the clump mass fraction  $f_{\text{clump}}$  and the mass range. Dalal & Kochanek (2002a) made a measurement of  $f_{\text{clump}}$  for a given clump mass, interpreting it as a weighted average over clump masses and an integral measure of small-scale power (Dalal & Kochanek 2002b). Further work is needed to understand how well studies of individual clumps in particular lens systems (e.g., Keeton 2001b) can provide a differential measure of the clump mass function and hence small-scale power. Even more importantly, the  $f_{\text{clump}}$  that matters for lensing is the fraction of the surface mass density in clumps, which may neither be independent of position nor represent a global clump mass fraction. The theory clearly needs to be further developed and explored before the claims from substructure lensing can be fully understood. For that to happen, it would be extremely helpful if we could find an analytic or semi-analytic approach to the theory.

One important aspect of the theory has until now been neglected. All previous studies of substructure lensing have assumed that the clumps lie in the halos of lens galaxies, which seems reasonable in light of known mass clumps in real galaxies (globular clusters, satellite galaxies, etc.) and predictions from CDM. However, as lensing is sensitive to all mass along the line of sight we should at least consider the possibility of clumps outside the galaxy. This issue has important bearing on the interpretation of substructure lensing. Low-mass halos form in both CDM and WDM (Warm Dark Matter) scenarios, but in WDM they are disrupted when they merge with larger halos (e.g., Colin et al. 2000; Knebe et al. 2002). Thus, if the clumps responsible for substructure lensing are in the lens galaxy halos, they argue strongly for CDM and against WDM (Dalal & Kochanek 2002a, 2002b). If they can be isolated,

<sup>1</sup> Hubble Fellow

however, their ability to rule out WDM may be weakened. Determining the relative importance of embedded and isolated clumps will require a detailed calculation of two effects: the number density of clumps in overdense regions like galaxies may be much higher than the number density of free-floating clumps (at least for CDM); but the portion of the line of sight that pierces the lens galaxy halo is a tiny fraction of the whole distance. That calculation is the focus of a separate paper (J. Chen et al., in preparation) based on the formalism and general results presented here.

This paper examines analytic aspects of substructure lensing, in part to understand general features of the effect, and to obtain simple analytic estimates of the lensing cross sections to facilitate future theoretical studies. Section 2 focuses on the case of a singular isothermal sphere (SIS) as a simple lens model that is a reasonable representation of cosmological objects and yet analytically tractable. Finch et al. (2002) recently gave a nice analysis of cross sections for multiple imaging for an SIS in an external shear. I extend their analysis by adding an external convergence and computing cross sections of interest for substructure lensing. Section 3 places clumps in the context of substructure lensing and considers for the first time the problem of clumps along the line of sight. I show that a clump at an arbitrary redshift is no more difficult to handle than a clump in the halo of the lens galaxy. Sections 2 and 3 are independent of each other, but Section 4 combines them to give quantitative examples for two observed lenses. Some readers may wish at first to skip Sections 2 and 3, which are rather technical, and start with the examples and discussion in Section 4. Finally, Section 5 offers conclusions.

## 2. SIS IN AN EXTERNAL FIELD

A singular isothermal sphere, with density profile  $\rho \propto r^{-2}$ , is a simple model that is often used in lensing because its simplicity permits detailed analytic treatment (e.g., Finch et al. 2002) and because it seems to be a good representation of the density profiles of galaxies on the 5–10 kpc scales relevant for strong lensing (e.g., Fabbiano 1989; Kochanek 1993; Maoz & Rix 1993; Kochanek 1996; Rix et al. 1997; Treu & Koopmans 2002). The model has been used to represent mass clumps for studies of substructure lensing, after taking into account tidal stripping by the parent halo (Metcalf & Madau 2001; Dalal & Kochanek 2002a). Again, the simplicity of the SIS makes it attractive for theoretical studies. For the  $\sim 10^6 M_\odot$  halos relevant for substructure lensing, the SIS profile does not differ dramatically from the NFW (Navarro, Frenk & White 1996) profile inferred from cosmological  $N$ -body simulations. If anything, SIS halos may be somewhat less concentrated than NFW halos, leading to slight underestimates of substructure lensing effects (see Metcalf & Madau 2001, especially their Figure 1). I study the SIS model because, given that it is at least moderately reasonable as a model, its analytic tractability makes it extremely valuable for theoretical studies of substructure lensing.

An SIS with velocity dispersion  $\sigma$  produces a deflection

$$\alpha(\mathbf{x}) = b \frac{\mathbf{x}}{|\mathbf{x}|}, \quad (1)$$

written as a two-component vector of angles on the sky. (See Schneider, Ehlers & Falco 1992 for an introduction to the SIS and lens theory in general.) The Einstein radius  $b$

is given by

$$b = 4\pi \left(\frac{\sigma}{c}\right)^2 \frac{D_{\text{ls}}}{D_{\text{os}}}, \quad (2)$$

where  $D_{\text{ls}}$  and  $D_{\text{os}}$  are angular diameter distances between the lens and source and the observer and source, respectively. (The distance ratio is the same for comoving distances.) In the presence of an external convergence  $\kappa$  and shear  $\gamma$ , the system is described by the lens equation

$$\mathbf{u} = (1 - \Gamma)\mathbf{x} - \alpha(\mathbf{x}), \quad (3)$$

$$\text{where } \Gamma = \begin{bmatrix} \kappa + \gamma & 0 \\ 0 & \kappa - \gamma \end{bmatrix}. \quad (4)$$

For convenience but without loss of generality, we are working in a coordinate system aligned with the shear. The lensing magnification  $\mu$  is given by

$$\mu^{-1} = \det\left(\frac{\partial \mathbf{u}}{\partial \mathbf{x}}\right) = \mu_0^{-1} - \frac{b}{r} [1 - \kappa - \gamma \cos 2\theta], \quad (5)$$

where

$$\mu_0 = \det(1 - \Gamma)^{-1} = [(1 - \kappa)^2 - \gamma^2]^{-1} \quad (6)$$

is the magnification produced by the background convergence and shear field in the absence of the SIS.

For substructure lensing we seek to understand how the lensing magnification is changed by the presence of the clump. In particular, we wish to know the cross section for the fractional difference between the magnification  $\mu$  with the clump and the magnification  $\mu_0$  without it to be  $\gtrsim 10$ –20%. To begin, note that there is a simple curve in the image plane with the property that all images on the curve have magnification  $\mu = (1 + \delta)\mu_0$ . Using eq. (5) we can write this curve parametrically as

$$r_\delta(\theta) = \frac{1 + \delta}{\delta} \mu_0 b [1 - \kappa - \gamma \cos 2\theta]. \quad (7)$$

Plugging  $r_\delta(\theta)$  into the lens equation yields a parametric form for the corresponding curve in the source plane,

$$\begin{aligned} u_\delta(\theta) &= [(1 - \kappa - \gamma)r_\delta(\theta) - b] \cos \theta, \\ v_\delta(\theta) &= [(1 - \kappa + \gamma)r_\delta(\theta) - b] \sin \theta. \end{aligned} \quad (8)$$

I refer to this as a “ $\delta$ -curve.” Note that the curve is defined only for values of  $\theta$  such that  $r_\delta(\theta) > 0$ . Also note that  $\delta$  is defined using the magnification  $\mu$  for a single image, not the total magnification  $\mu_{\text{tot}} = \sum_i |\mu_i|$ ; the difference will become important below.

The critical curve and caustic can be found by taking the limit  $\delta \rightarrow \infty$ . Finally, the pseudo-caustic is the curve in the source plane that maps to the origin in the image plane (see Evans & Wilkinson 1998), which can be written parametrically as

$$\begin{aligned} u_p(\theta) &= -b \cos \theta, \\ v_p(\theta) &= -b \sin \theta. \end{aligned} \quad (9)$$

We must now distinguish between three cases based on the values of  $\kappa$  and  $\gamma$ .

### 2.1. Positive global parity

The three cases are distinguished by the two eigenvalues  $\lambda_\pm = 1 - \kappa \pm \gamma$  of the tensor  $(1 - \Gamma)$ . The first case is when  $\kappa$  and  $\gamma$  are small enough that both eigenvalues are positive, or  $\kappa + \gamma < 1$ . An image produced by the external field alone (without the SIS) would have positive parity.

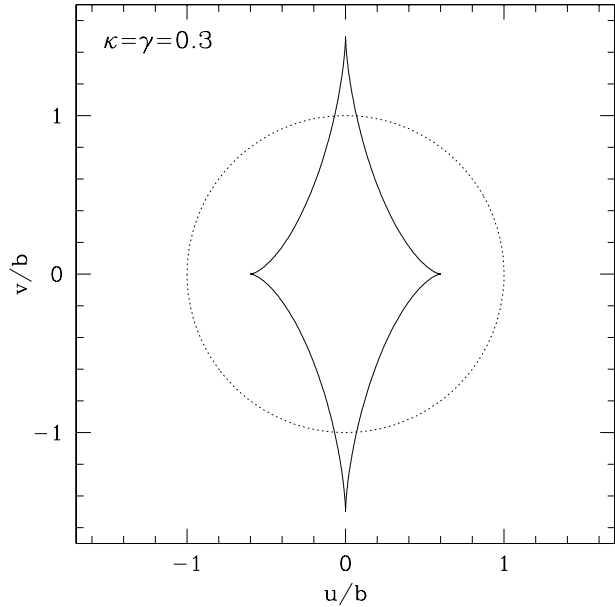


FIG. 1.— Caustic (solid) and pseudo-caustic (dotted) for an SIS in an external field with  $\kappa = \gamma = 0.3$  and hence positive global parity. The axes are labeled in units of the SIS Einstein radius,  $b$ .

Figure 1 shows an example of the caustic and pseudo-caustic for this case. The caustic generically has an “astroid” shape. If  $\gamma$  is small the caustic is completely enclosed by the pseudo-caustic, and the system has standard one, two, and four-image configurations. For larger  $\gamma$  such that  $3\gamma + \kappa > 1$  (as in the example), the caustic pierces the pseudo-caustic and produces “naked cusps” that correspond to an image configuration with three bright images (e.g., Kassiola & Kovner 1993).

Figure 2 shows examples of  $\delta$ -curves (from eq. 8). With positive global parity the curves exist only for  $\delta > 0$ , and each one is valid for all  $0 \leq \theta \leq 2\pi$ . In general the curves have a two-lobed shape that extends far along the vertical axis. There is a very large region where the magnification is 10–20% larger than the background value ( $\delta = 0.1$ – $0.2$ ), which is more than an order of magnitude larger than the caustics.

The area enclosed by a  $\delta$ -curve can be computed from the parametric form as

$$A(\delta; \kappa, \gamma) = \int_0^{2\pi} \frac{1}{2} \left[ \mathbf{u}_\delta(\theta) \times \frac{d\mathbf{u}_\delta}{d\theta} \right] d\theta, \quad (10)$$

where  $d\mathbf{u}_\delta/d\theta$  is the parametric derivative, and  $\times$  indicates the vector cross product. Geometrically, the integrand is the area of the triangle defined by the origin and the points  $\mathbf{u}_\delta(\theta)$  and  $\mathbf{u}_\delta(\theta + d\theta)$ , and the integral simply sums all of the triangles. The integral can be evaluated analytically,

$$A(\delta; \kappa, \gamma) = \frac{\pi b^2}{2\delta^2} \frac{2(1 - \kappa)^2 + (1 - 3\delta^2)\gamma^2}{(1 - \kappa)^2 - \gamma^2}. \quad (11)$$

Incidentally, in the limit  $\delta \rightarrow \infty$  this analysis gives the area inside the caustic as  $(3/2)\pi b^2 \gamma^2 \mu_0$ , which is a trivial generalization to  $\kappa \neq 0$  of the result given by Finch et al. (2002).

Consider the  $\delta$ -curve for some given value  $\delta$ . The area within the curve is filled by other  $\delta$ -curves with  $\delta' > \delta$ .

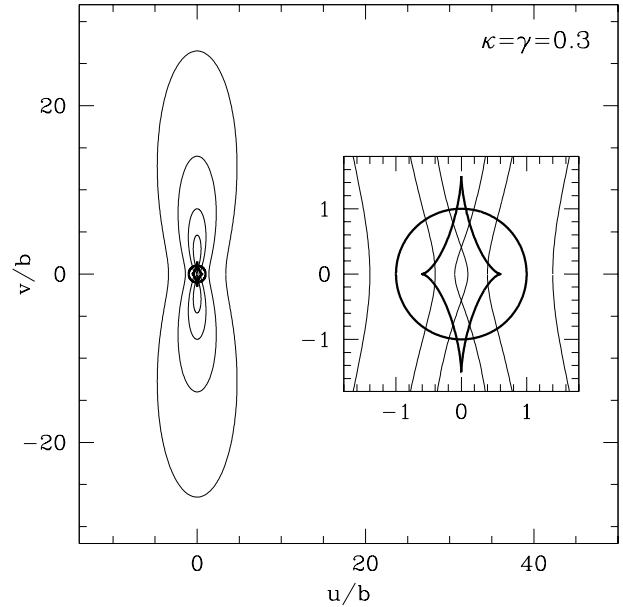


FIG. 2.— The light lines show  $\delta$ -curves in the source plane, with  $\delta = (0.1, 0.2, 0.4, 0.8)$  from the outside moving in. The heavy lines in the middle show the caustic and pseudo-caustic from Figure 1. The inset shows a close-up of the region near the origin.

Thus, the curve encloses a region where the magnification perturbation  $\mu/\mu_0 - 1$  is at least as large as  $\delta$ . Consequently,  $A(\delta; \kappa, \gamma)$  is a lower limit on the cross section for a magnification perturbation stronger than  $\delta$ . To understand why it is only a lower limit, recall that  $\delta = \mu/\mu_0 - 1$  is defined using the magnification  $\mu$  for a single image (the image lying on the curve in the image plane defined by eq. 7) — not the total magnification  $\mu_{\text{tot}} = \sum_i |\mu_i|$ . Since  $\mu_{\text{tot}} \geq \mu$ , we have  $\delta_{\text{tot}} \geq \delta$ . This detail is unimportant if the  $\delta$ -curve lies entirely outside the caustic and pseudo-caustic, which is true for

$$\delta < \frac{1 - \kappa - \gamma}{1 - \kappa + 3\gamma}, \quad (12)$$

because then all points on the  $\delta$ -curve are singly-imaged so  $\mu_{\text{tot}} = \mu$  and  $\delta_{\text{tot}} = \delta$ . However, if eq. (12) is violated then there is a region outside the  $\delta$ -curve but inside the caustic and/or pseudo-caustic where  $\delta_{\text{tot}} > \delta$  (see the inset of Figure 2), so the cross section for a *total* magnification perturbation stronger than  $\delta$  is somewhat larger than  $A(\delta; \kappa, \gamma)$ . Nevertheless, in many cases the  $\delta$ -curve is so much larger than the caustic and pseudo-caustic that the additional area is negligible, so  $A(\delta; \kappa, \gamma)$  should still be a good approximation to the desired cross section.

To test the approximation, I compute the exact cross section numerically. For a given source I solve the lens equation numerically (using the algorithm and software from Keeton 2001a) to find all of the images and compute the total magnification. I use this process to map the magnification as a function of source position, and then compute the cross section. Figure 3 compares the exact numerical cross section to the analytic estimate. When eq. (12) is satisfied the analytic result is exact; when it is violated the analytic result is indeed a lower limit on the cross section, and a very good approximation provided the cross section is larger than a few times  $\pi b^2$ . Even when

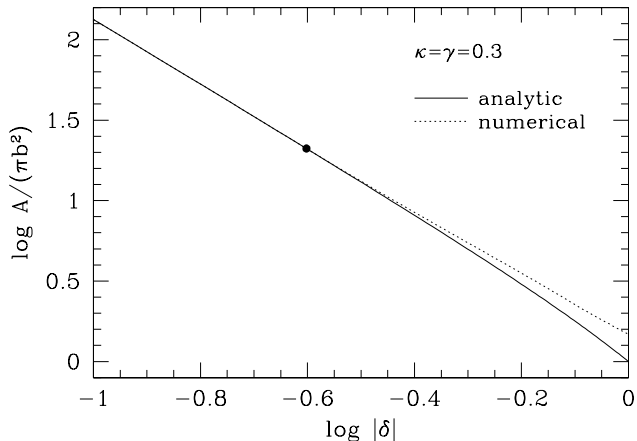


FIG. 3.— Estimates of the cross section for a magnification perturbation stronger than  $\delta$ , in units of the area  $\pi b^2$  within the Einstein ring. The dotted curve shows the exact value computed by numerically solving the lens equation (see text), while the solid curve shows the analytic estimate from eq. (11). The analytic result is exact to the left of the dot (see eq. 12).

the approximation is mediocre, having a simple lower limit on the cross section is still very useful.

## 2.2. Negative global parity

In the second class of problems the eigenvalues of  $(1 - \Gamma)$  have different signs, with  $1 - \kappa - \gamma < 0$  and  $1 - \kappa + \gamma > 0$ . An image produced by the external field alone (without the SIS) would have negative parity.

Figure 4 shows an example of the caustic and pseudo-caustic for this case, and Figure 5 shows  $\delta_{\text{tot}} = |\mu_{\text{tot}}/\mu_0| - 1$  as a function of position along the axes. The caustic lies outside the pseudo-caustic and does not close on itself but instead closes where it touches the pseudo-caustic, at the parameter value such that  $\cos 2\theta = (1 - \kappa)/\gamma$ . A source outside both caustics produces one image with negative parity. A source inside the pseudo-caustic produces two images, and both have negative parity;<sup>2</sup> despite having two images, the total magnification is still smaller than the background value ( $\delta_{\text{tot}} < 0$ ; see Figure 5). A source between the caustic and pseudo-caustic produces three images, one with positive parity and two with negative parity. The area of the pseudo-caustic is  $\pi b^2$ , and the area between the pseudo-caustic and caustic is

$$A_c = -\frac{\mu_0 b^2}{2} \left\{ -3(1 - \kappa)[-(1 - \kappa)^2 + \gamma^2]^{1/2} + [2(1 - \kappa)^2 + \gamma^2] \cos^{-1} \left( \frac{1 - \kappa}{\gamma} \right) \right\}, \quad (13)$$

where  $\mu_0$  is given by eq. (6), and we have  $\mu_0 < 0$  for negative global parity.

Figure 6 shows examples of  $\delta$ -curves for this case. With negative global parity the curves exist for both  $\delta > 0$  and  $\delta < 0$ , but each has a finite range of the parameter  $\theta$ :

$$\begin{aligned} \delta > 0 : \cos 2\theta &\geq \frac{1 - \kappa}{\gamma}, \\ \delta < 0 : \cos 2\theta &\leq \frac{1 - \kappa}{\gamma}. \end{aligned} \quad (14)$$

<sup>2</sup> This contrasts with the case of positive global parity, where a source inside the pseudo-caustic produces one positive-parity image and one negative-parity image.

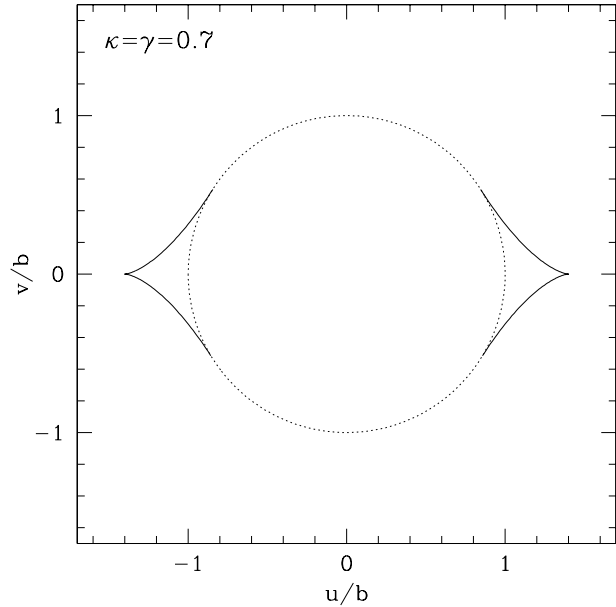


FIG. 4.— Caustic (solid) and pseudo-caustic (dotted) for an SIS in an external field with  $\kappa = \gamma = 0.7$  and hence negative global parity.

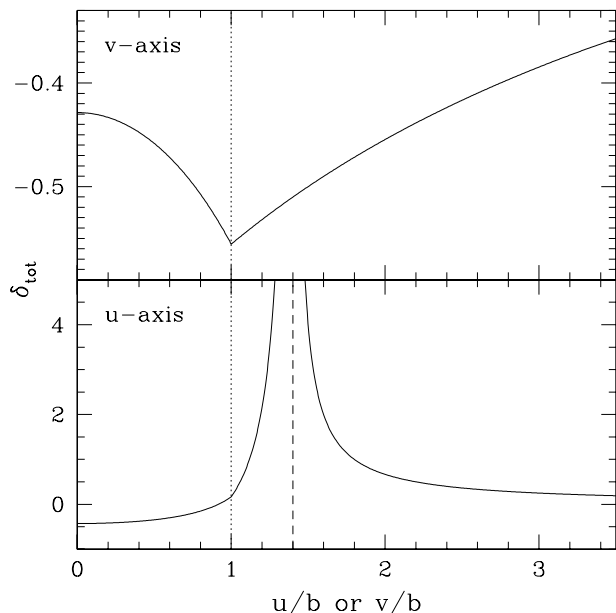


FIG. 5.— Total magnification perturbation  $\delta_{\text{tot}}$  as a function of position along the axes in Figure 4. The vertical dotted line marks the position of the pseudo-caustic, while the vertical dashed line marks the cusp of the caustic on the  $u$ -axis.

The  $\delta > 0$  curves have two disjoint lobes that extend to moderate distances along the horizontal axis, while the  $\delta < 0$  curves extend to large distances along the vertical axis. In other words, for negative global parity there is a moderate-sized region where the magnification is enhanced relative to the background value, plus a large region where the magnification is *reduced*.

A close-up of the region near the origin shows that the  $\delta$ -curves intersect themselves (inside the caustic in the inset

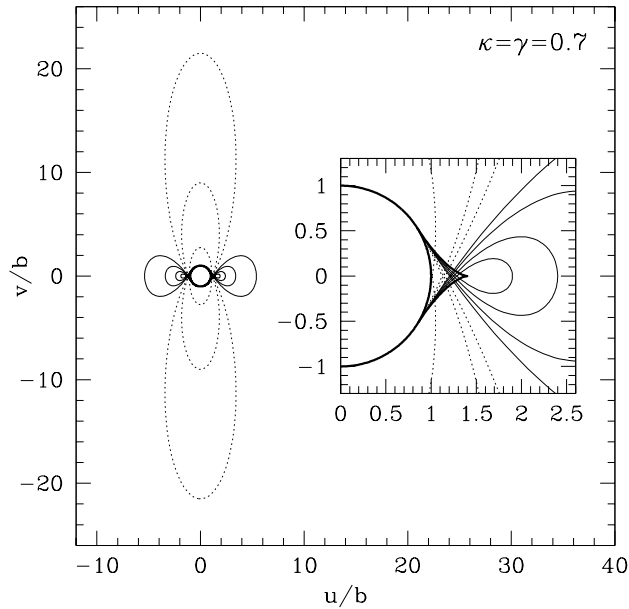


FIG. 6.— The light lines show  $\delta$ -curves in the source plane; the solid lines have  $\delta = (0.1, 0.2, 0.4, 0.8)$ , while the dotted lines have  $\delta = (-0.1, -0.2, -0.4)$ . The heavy lines in the middle show the caustic and pseudo-caustic from Figure 4. The inset shows a close-up of the region near the origin.

of Figure 6); the intersection occurs at the parameter value

$$\theta_\delta = \sin^{-1} \left[ -\frac{1 - \kappa - \gamma}{2\gamma(1 + \delta)} \right]^{1/2}. \quad (15)$$

Recall that  $1 - \kappa - \gamma < 0$ , so the term in square brackets is positive. Note that this term exceeds unity when

$$\delta < -\frac{1 - \kappa + \gamma}{2\gamma} < 0, \quad (16)$$

in which case this formalism breaks down. This happens only for large negative  $\delta$ , at positions deep inside the pseudo-caustic where the  $\delta$ -curve formalism does not accurately represent the cross section, for cases where the cross section is small and uninteresting anyway. So this is not a concern for most  $\delta < 0$  cases of interest, and we can compute the enclosed area as

$$\begin{aligned} A_-(\delta; \kappa, \gamma) &= 2 \int_{\theta_\delta}^{\pi - \theta_\delta} \frac{1}{2} \left[ \mathbf{u}_\delta(\theta) \times \frac{d\mathbf{u}_\delta}{d\theta} \right] d\theta, \\ &= -\frac{\mu_0 b^2}{2\delta^2} \left\{ (\pi - 2\theta_\delta) [2(1 - \kappa)^2 + (1 - 3\delta^2)\gamma^2] \right. \\ &\quad \left. - f(\delta; \kappa, \gamma) \right\}, \end{aligned} \quad (17)$$

where the integral covers one lobe, the leading factor of two counts the other lobe, and

$$\begin{aligned} f(\delta; \kappa, \gamma) &= \frac{1}{1 + \delta} [1 - \kappa + \gamma(1 + 2\delta)]^{1/2} (-1 + \kappa + \gamma)^{1/2} \\ &\quad \times [\gamma\delta(1 + 3\delta) - (3 + \delta)(1 - \kappa)]. \end{aligned} \quad (18)$$

Eq. (17) is the area where the magnification perturbation for one image is stronger than  $\delta$  (by which I mean  $|\mu/\mu_0| - 1 < \delta$  since  $\delta < 0$ ). It is only an approximation to the area where the total magnification perturbation is stronger than  $\delta$ , because of the difference between  $\delta$  and

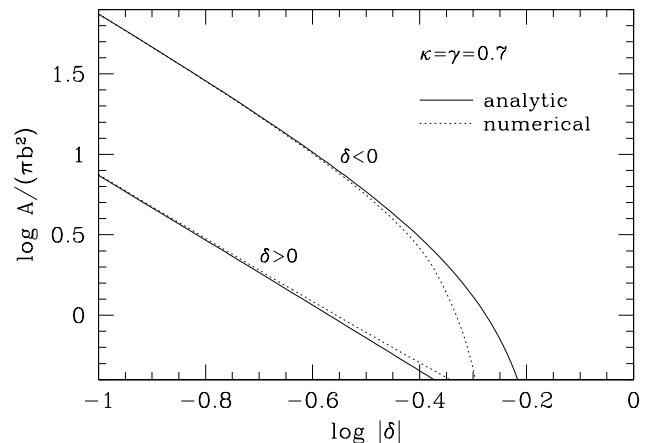


FIG. 7.— Estimates of the cross section for a magnification perturbation stronger than  $\delta$ . Dotted curves show exact values computed by numerically solving the lens equation (see text), while solid curves show analytic estimate from eqs. (17) and (19).

$\delta_{\text{tot}}$  inside the caustic and pseudo-caustic. However, Figure 7 compares the analytic result with an exact numerical evaluation of the cross section (see §2.1 for details) and shows that the approximation is very good provided the cross section is larger than a few times  $\pi b^2$ .

A  $\delta$ -curve with  $\delta > 0$  always has two disjoint lobes with total area

$$\begin{aligned} A_+(\delta; \kappa, \gamma) &= 2 \int_{-\theta_\delta}^{\theta_\delta} \frac{1}{2} \left[ \mathbf{u}_\delta(\theta) \times \frac{d\mathbf{u}_\delta}{d\theta} \right] d\theta, \\ &= -\frac{\mu_0 b^2}{2\delta^2} \left\{ 2\theta_\delta [2(1 - \kappa)^2 + (1 - 3\delta^2)\gamma^2] \right. \\ &\quad \left. + f(\delta; \kappa, \gamma) \right\}, \end{aligned} \quad (19)$$

where again the integral covers one lobe, the leading factor of two counts the other lobe, and  $f(\delta; \kappa, \gamma)$  is given by eq. (18). This is a lower limit on the area where the total magnification perturbation is stronger than  $\delta$ , because it omits some area inside the caustic where  $\mu_{\text{tot}} > \mu$  and  $\delta_{\text{tot}} > \delta$ . Figure 7 shows, though, that the analytic result is a very good approximation to the exact numerical cross section.

### 2.3. Doubly negative global parity

In the final class of problems the eigenvalues of  $(1 - \Gamma)$  are both negative,  $1 - \kappa - \gamma < 0$  and  $1 - \kappa + \gamma < 0$ . In real lenses this case occurs only for an image very near the center of the lens galaxy, where the high surface density leads to strong demagnification. Observations of such “core” images are very rare (e.g., Rusin & Ma 2001; Keeton 2002), so in practice this case is unimportant for studies of substructure lensing.

## 3. SUBSTRUCTURE LENSING

I now turn to the case of substructure lensing, in which a small clump lies along the line of sight to one of the images in a strong lens system. On the scale of the clump — for realistic situations the characteristic clump Einstein radius is  $\sim 1$  mas (e.g., Dalal & Kochanek 2002a) — the effect of the main lens galaxy can be approximated as a simple convergence and shear. In this section I manipulate

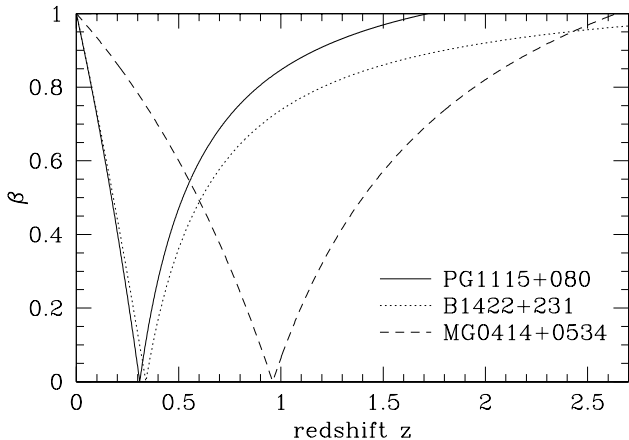


FIG. 8.—  $\beta$  versus the clump redshift, for three lens systems: PG 1115+080 with  $z_s = 1.72$  and  $z_l = 0.31$ ; B1422+231 with  $z_s = 3.62$  and  $z_l = 0.34$ ; and MG 0414+0534 with  $z_s = 2.64$  and  $z_l = 0.96$  (Weymann et al. 1980; Patnaik et al. 1992; Lawrence et al. 1995; Kundić et al. 1997a, 1997b; Tonry & Kochanek 1999). The cosmology is  $\Omega_M = 0.3$  and  $\Omega_\Lambda = 0.7$ .

the lens equation to map the galaxy+clump problem onto the simpler problem of a clump in an external field. The analysis in this section is general and does not assume any specific form for either the galaxy or the clump.

The clump may be embedded in the halo of the main lens galaxy, but for generality I also consider the possibility that it lies elsewhere along the line of sight. This requires formulating the lens equation with two lens planes. Suppose a deflector at redshift  $z_1$  produces deflection  $\alpha_1(\mathbf{x})$ , and a second deflector at redshift  $z_2 \geq z_1$  produces deflection  $\alpha_2(\mathbf{x})$ . The lens equation then has the form (e.g., Schneider et al. 1992)

$$\mathbf{u} = \mathbf{x} - \alpha_1(\mathbf{x}) - \alpha_2[\mathbf{x} - \beta\alpha_1(\mathbf{x})], \quad (20)$$

where the factor

$$\beta = \frac{D_{12}D_{os}}{D_{o2}D_{1s}} \quad (21)$$

encodes the redshift difference in terms of a distance ratio,<sup>3</sup> where  $D_{ij} = D(z_i, z_j)$  and “o” and “s” refer to the observer and source respectively. Figure 8 shows that  $\beta$  vanishes if the two redshifts are the same, and monotonically approaches unity as either redshift approaches the observer or the source. Given the form of eq. (20), we must distinguish between cases where the clump is in the foreground or background of the galaxy. The case of a clump embedded in the galaxy is given by the limit  $\beta \rightarrow 0$  of either case.

### 3.1. Foreground clump

Let  $\alpha_g(\mathbf{x})$  be the deflection of the galaxy<sup>4</sup> without the clump and  $\alpha_c(\mathbf{x})$  be the deflection from the clump in question. Suppose that without the clump the galaxy takes a source at position  $\mathbf{u}$  and produces an image at position  $\mathbf{x}_0$ , so the unperturbed lens equation is

$$\mathbf{u} = \mathbf{x}_0 - \alpha_g(\mathbf{x}_0). \quad (22)$$

<sup>3</sup> The distance ratio is the same for angular diameter distances or comoving distances.

<sup>4</sup> The “galaxy” may be smooth, but it could also include other clumps that are far from the clump in question. It may also include any external tidal shear from large objects near the lens galaxy. In the language of substructure lensing, it represents the macromodel.

With the clump present, the lens takes the same source to an image at  $\mathbf{x}$  given by the perturbed lens equation (compare eq. 20)

$$\mathbf{u} = \mathbf{x} - \alpha_c(\mathbf{x} - \mathbf{x}_c) - \alpha_g[\mathbf{x} - \beta\alpha_g(\mathbf{x})], \quad (23)$$

for a clump in the foreground of the galaxy. Note that we write  $\alpha_c(\mathbf{x} - \mathbf{x}_c)$  to emphasize that the clump deflection depends only on the position relative to the clump center  $\mathbf{x}_c$ . Subtracting eqs. (22) and (23), we find an equation relating  $\mathbf{x}_0$  and  $\mathbf{x}$ ,

$$0 = (\mathbf{x} - \mathbf{x}_0) - \{\alpha_g[\mathbf{x} - \beta\alpha_c(\mathbf{x})] - \alpha_g(\mathbf{x}_0)\} - \alpha_c(\mathbf{x} - \mathbf{x}_c). \quad (24)$$

If the clump is small relative to the galaxy such that the perturbation  $\mathbf{x} - \mathbf{x}_0$  is small relative to length scales associated with the galaxy, then we can expand  $\alpha_g(\mathbf{x})$  in a Taylor series and write

$$\alpha_g(\mathbf{x}) = \alpha_g(\mathbf{x}_0) + \Gamma \cdot (\mathbf{x} - \mathbf{x}_0), \quad (25)$$

$$\text{where } \Gamma \equiv \begin{bmatrix} \frac{\partial\alpha_{gx}}{\partial x} & \frac{\partial\alpha_{gx}}{\partial y} \\ \frac{\partial\alpha_{gy}}{\partial x} & \frac{\partial\alpha_{gy}}{\partial y} \end{bmatrix}, \quad (26)$$

where the derivatives in  $\Gamma$  are evaluated at the unperturbed image position  $\mathbf{x}_0$ . In the language of substructure lensing,  $\Gamma$  represents the convergence and shear from the macromodel. Using eq. (25) in eq. (24) yields

$$0 = (1 - \Gamma)(\mathbf{x} - \mathbf{x}_0) - (1 - \beta\Gamma)\alpha_c(\mathbf{x} - \mathbf{x}_c). \quad (27)$$

Now define  $\mathbf{y} = \mathbf{x} - \mathbf{x}_c$  as a coordinate system centered on the clump position, and multiply eq. (27) on the left by  $(1 - \beta\Gamma)^{-1}$  to obtain

$$\mathbf{u}_{\text{eff}} = (1 - \Gamma_{\text{eff}})\mathbf{y} - \alpha_c(\mathbf{y}), \quad (28)$$

where

$$\mathbf{u}_{\text{eff}} \equiv -(1 - \beta\Gamma)^{-1}(1 - \Gamma)(\mathbf{x}_c - \mathbf{x}_0), \quad (29)$$

$$\Gamma_{\text{eff}} \equiv 1 - (1 - \beta\Gamma)^{-1}(1 - \Gamma). \quad (30)$$

Eq. (28) has the same form as eq. (3), so we have mapped the general line-of-sight clump problem onto an equivalent problem of a clump in a simple external field, where the effective convergence and shear are

$$\kappa_{\text{eff}} = \frac{(1 - \beta)[\kappa - \beta(\kappa^2 - \gamma^2)]}{(1 - \beta\kappa)^2 - (\beta\gamma)^2}, \quad (31)$$

$$\gamma_{\text{eff}} = \frac{(1 - \beta)\gamma}{(1 - \beta\kappa)^2 - (\beta\gamma)^2}. \quad (32)$$

Note that the ratio  $\mu/\mu_0$  is the same for the general line-of-sight clump problem and the equivalent clump plus external field problem, so  $\delta$  is the same for both problems. Taking advantage of the mapping to the simpler problem, we can write the cross section  $\sigma$  for a magnification perturbation stronger than  $\delta$  as

$$\begin{aligned} \sigma(\delta; \kappa, \gamma, \beta) &= \int f_\delta d\mathbf{x}_c = \int f_\delta \left| \frac{\partial\mathbf{x}_c}{\partial\mathbf{u}_{\text{eff}}} \right| d\mathbf{u}_{\text{eff}} \\ &= \left| \frac{\det(1 - \beta\Gamma)}{\det(1 - \Gamma)} \right| A(\delta; \kappa_{\text{eff}}, \gamma_{\text{eff}}), \end{aligned} \quad (33)$$

where  $f_\delta$  is unity if the clump position  $\mathbf{x}_c$  corresponds to a perturbation stronger than  $\delta$ , and zero otherwise. In other words, the cross section for the general line-of-sight clump problem is simply a multiplicative factor times the cross section for the equivalent clump plus external field problem. For an SIS clump,  $A(\delta; \kappa_{\text{eff}}, \gamma_{\text{eff}})$  is given by eq. (11), (17), or (19).

It is important to remark on the parity. The parity of the equivalent problem is given by

$$1 - \kappa_{\text{eff}} - \gamma_{\text{eff}} = \frac{1 - \kappa - \gamma}{1 - \beta(\kappa + \gamma)}. \quad (34)$$

If the global parity in the full problem is positive ( $1 - \kappa - \gamma > 0$ ), then the parity of the equivalent problem is always positive ( $1 - \kappa_{\text{eff}} - \gamma_{\text{eff}} > 0$ ). However, if the global parity in the full problem is negative ( $1 - \kappa - \gamma < 1$  and  $1 - \kappa + \gamma > 0$ ), then the parity of the effective problem can be either negative or positive depending on the value of  $\beta$ :

$$1 - \kappa_{\text{eff}} - \gamma_{\text{eff}} = \begin{cases} < 0, & \beta < (\kappa + \gamma)^{-1} \\ > 0, & \beta > (\kappa + \gamma)^{-1} \end{cases} \quad (35)$$

This is an important detail for clumps that lie along the line of sight but far in redshift from a lensed image with negative parity, as we shall see in §4.

### 3.2. Background clump

For a clump in the background of the galaxy, the perturbed lens equation is

$$\mathbf{u} = \mathbf{x} - \alpha_g(\mathbf{x}) - \alpha_c[\mathbf{x} - \beta\alpha_g(\mathbf{x}) - \mathbf{x}_c]. \quad (36)$$

Again subtracting the unperturbed lens equation eq. (22) and using eq. (25) to approximate  $\alpha_g(\mathbf{x})$ , we find the equation relating  $\mathbf{x}_0$  and  $\mathbf{x}$  to be

$$0 = (1 - \Gamma)(\mathbf{x} - \mathbf{x}_0) - \alpha_c[(1 - \beta\Gamma)(\mathbf{x} - \mathbf{x}_0) + \mathbf{x}_0 - \beta\alpha_g(\mathbf{x}_0) - \mathbf{x}_c]. \quad (37)$$

Changing variables to

$$\mathbf{y} = (1 - \beta\Gamma)(\mathbf{x} - \mathbf{x}_0) + \mathbf{x}_0 - \beta\alpha_g(\mathbf{x}_0) - \mathbf{x}_c, \quad (38)$$

we find

$$\mathbf{u}_{\text{eff}} = (1 - \Gamma_{\text{eff}})\mathbf{y} - \alpha_c(\mathbf{y}), \quad (39)$$

where

$$\mathbf{u}_{\text{eff}} \equiv -(1 - \Gamma)(1 - \beta\Gamma)^{-1}[\mathbf{x}_c - \mathbf{x}_0 + \beta\alpha_g(\mathbf{x}_0)], \quad (40)$$

$$\Gamma_{\text{eff}} \equiv 1 - (1 - \Gamma)(1 - \beta\Gamma)^{-1}. \quad (41)$$

We have again mapped the general line-of-sight clump problem onto the simple problem of a clump in an external field, where the effective convergence and shear are again given by eqs. (31) and (32). The cross section for a magnification perturbation stronger than  $\delta$  is then

$$\begin{aligned} \sigma(\delta; \kappa, \gamma, \beta) &= \int f_\delta d\mathbf{x}_c = \int f_\delta \left| \frac{\partial \mathbf{x}_c}{\partial \mathbf{u}_{\text{eff}}} \right| d\mathbf{u}_{\text{eff}} \\ &= \left| \frac{\det(1 - \beta\Gamma)}{\det(1 - \Gamma)} \right| A(\delta; \kappa_{\text{eff}}, \gamma_{\text{eff}}), \end{aligned} \quad (42)$$

so again the cross section for the general line-of-sight clump problem is simply a multiplicative factor times the cross section for the equivalent clump plus external field problem. The parity comments from the end of §3.1 apply here as well. Note that the foreground and background clump cases involve different manipulations of the lens equation but arrive at the same mapping of the line-of-sight clump problem to the clump plus external field problem (eqs. 33 and 42).

## 4. SAMPLE SIS CROSS SECTIONS

### 4.1. Procedure

If we assume SIS clumps, we can combine results from the previous two sections to make quantitative estimates of cross sections for substructure lensing in real lenses. The procedure is as follows.

- Select a lens and get the source and lens redshifts. Select one image and get values for  $\kappa$  and  $\gamma$  from a smooth macromodel.
- Choose a perturbation threshold  $\delta$ , guided by data. For example, if the observed flux is 20% fainter than predicted by smooth models then one would set  $\delta = -0.2$  to estimate the probability that substructure produces an effect at least as strong as observed. Alternatively, if all other statistical and systematic effects are thought to be smaller than 20% then one could set  $\delta = \pm 0.2$  to estimate the probability of a noticeable substructure effect.
- Pick a redshift for the clump and compute  $\beta$ .
- Use eqs. (31) and (32) to compute  $\kappa_{\text{eff}}$  and  $\gamma_{\text{eff}}$ , mapping the original problem to the equivalent problem of a clump in an external field. Compute the effective cross section using results from §2, where the parity and sign of  $\delta$  determine which formula is appropriate:
 
$$1 - \kappa_{\text{eff}} - \gamma_{\text{eff}} > 0 : \quad A(\delta; \kappa_{\text{eff}}, \gamma_{\text{eff}}) = \begin{cases} \text{eq. (11)} & \delta > 0 \\ 0 & \delta < 0 \end{cases} \quad (43)$$

$$1 - \kappa_{\text{eff}} - \gamma_{\text{eff}} < 0 : \quad A(\delta; \kappa_{\text{eff}}, \gamma_{\text{eff}}) = \begin{cases} \text{eq. (17)} & \delta < 0 \\ \text{eq. (19)} & \delta > 0 \end{cases} \quad (44)$$
- Use eq. (33) to convert back to the cross section for the original problem.

### 4.2. Data

I consider two systems that seem to require substructure lensing. B1422+231 is a radio-loud quasar at redshift  $z_s = 3.62$  lensed into four images by an early-type galaxies in a poor group of galaxies at redshift  $z_l = 0.34$  (Patnaik et al. 1992; Kundić et al. 1997b; Tonry 1998). Images A and C are bright positive-parity images, while B is a bright negative-parity image and D is a faint negative-parity image. In the geometric language used by Schechter & Wambsganss (2002), A and C lie at minima of the time delay surface, while B and D lie at saddlepoints.<sup>5</sup> Table 1 gives the convergence and shear from macromodels of the system. The image positions can be fit to high precision, but the flux ratios have long been a problem (e.g., Hogg & Blandford 1994; Kormann, Schneider & Bartelmann 1994; Keeton, Kochanek & Seljak 1997; Mao & Schneider 1998; Bradač et al. 2002; Metcalf & Zhao 2002). Keeton (2001b) argues that there must be a clump lying in front of image A with mass  $10^{5-6} M_\odot$  if it is a point mass, or  $10^{6-7} M_\odot$  if it is an SIS.

<sup>5</sup> There is presumably a faint fifth image lying at a maximum of the time delay surface near the center of the lens galaxy, which would have doubly negative parity, but if it exists it is too faint to have been observed (Patnaik et al. 1992).

PG 1115+080 is a radio-quiet quasar at  $z_s = 1.72$  lensed into four images by an early-type galaxy in a poor group of galaxies at redshift  $z_l = 0.31$  (Weymann et al. 1980; Kundić et al. 1997a; Tonry 1998). Images A<sub>1</sub> and C are positive-parity images (minima), while A<sub>2</sub> and B are negative-parity images (saddlepoints). Again the image positions can be fit to high precision, but the observed A<sub>2</sub>/A<sub>1</sub> flux ratio of  $\sim 0.65$  is hard to reconcile with a generic prediction of  $\sim 0.96$  for smooth macromodels (e.g., Impey et al. 1998; Metcalf & Zhao 2002).

#### 4.3. Results

Figure 9 shows the estimated cross sections for an SIS clump embedded in the lens galaxy, as a function of  $\delta$ , for each image in the two systems. In B1422+231 there is a substantial cross section for the positive-parity images A and C to be made *brighter* by substructure ( $\delta > 0$ ). There is a smaller cross section for negative-parity image B to be likewise enhanced, but a much more significant cross section for it to be made *dimmer* ( $\delta < 0$ ). The faint negative-parity image D is much less likely to be affected, and due to its faintness it is more likely to be brightened than dimmed. The results for PG 1115+080 are similar: positive-parity images (A<sub>1</sub> and C) are always brightened by an SIS clump, while negative-parity images (A<sub>2</sub> and B) can be brightened but are much more likely to be suppressed. The differences between positive-parity images and negative-parity images are similar to those discussed by Schechter & Wambsganss (2002). Although those authors were studying microlensing (perturbations by point-mass stars), the qualitative features are similar because the conceptual differences between SIS and point-mass clumps are small.

Figure 10 shows how the cross sections change if the clump is taken out of the lens galaxy and placed elsewhere along the line of sight. In general the cross sections peak at the redshift of the lens galaxy, but the curves are relatively broad with a FWHM of  $\Delta z \sim 0.11$ – $0.34$ . In other

TABLE 1

| Lens        | Image          | $\kappa$ | $\gamma$ | $\mu_0$ |
|-------------|----------------|----------|----------|---------|
| B1422+231   | A              | 0.384    | 0.476    | 6.57    |
|             | B              | 0.471    | 0.634    | −8.26   |
|             | C              | 0.364    | 0.414    | 4.29    |
|             | D              | 1.863    | 2.025    | −0.30   |
| PG 1115+080 | A <sub>1</sub> | 0.532    | 0.412    | 19.96   |
|             | A <sub>2</sub> | 0.551    | 0.504    | −19.10  |
|             | B              | 0.663    | 0.644    | −3.32   |
|             | C              | 0.469    | 0.286    | 5.00    |

Note. — Convergences, shears, and magnifications from macromodels. B1422+231 is modeled as a singular isothermal ellipsoid (SIE) plus an external shear (Keeton 2001b), while PG 1115+080 is modeled as an SIE plus an additional SIS representing the surrounding poor group of galaxies (Impey et al. 1998).

words, clumps could differ in redshift from the lens galaxy by up to several tenths and still have a significant effect on the images. For positive-parity images, the cross section for brightening ( $\delta > 0$ ) even has tails extending to  $z = 0$  and to the source redshift. For negative-parity images, the cross section for dimming ( $\delta < 0$ ) is broad but falls to zero at the redshifts where  $\beta > (\kappa + \gamma)^{-1}$  (see eq. 35). The cross section for brightening ( $\delta > 0$ ) of negative-parity images is actually a *minimum* at the lens redshift and increases moving toward  $z = 0$  or the source redshift. Although conceptually interesting, this behavior may not be of practical importance because the  $\delta > 0$  cross section tends to be much smaller than the corresponding  $\delta < 0$  cross section for a negative-parity image.

These results reveal the interesting possibility that clumps at a range of redshifts can have a substantial effect on lensing. The clumps need not be associated with the lens galaxies but could be the sort of isolated small halos predicted to be common in hierarchical structure formation models. It is not known whether isolated clumps are likely to be important in practice. Although their number per unit volume is expected to be much lower than that for embedded clumps in overdense regions like galaxies (at least for CDM), they are viable for lensing over a much larger volume. Determining the relative importance of the two populations will involve a detailed calculation combining lensing cross sections with appropriate clump mass functions (J. Chen et al., in preparation). The question is significant because if isolated clumps cannot be ignored, they will weaken the argument that substructure lensing opposes a Warm Dark Matter model (see §1).

#### 4.4. Comments

So far this analysis has considered only a single clump, but it can be extended to a clump population if we make the assumption that the optical depth is low enough that the clumps essentially act independently. In this case, the optical depth due to clumps in a patch of sky is estimated by summing the cross sections of all clumps in the patch and dividing by the area of the patch,

$$\tau(\delta; \kappa, \gamma) = \int_0^{z_s} dz D(z)^2 \frac{dD}{dz} \int dM \frac{dn}{dM} \sigma(\delta; \kappa, \gamma, \beta, M), \quad (45)$$

where  $\sigma$  is the cross section for a single clump,  $dn/dM$  is the mass function of clumps, and  $D(z)$  is the comoving distance. The optical depth is independent of the area of the patch provided that the number density of clumps is constant across the patch. The assumption that the clumps act independently can be checked *a posteriori* by seeing whether the estimated optical depth is small. If so, the assumption is valid. If not, the estimated optical depth may not be accurate — but it is still useful, because it at least indicates that the optical depth is not vanishingly small. That alone may be sufficient for some questions, such as the importance of isolated clumps. In any case, a numerical evaluation of the double integral in eq. (45) is much faster than a Monte Carlo or ray shooting simulation of lensing with clumps, so it should be valuable for exploring the optical depth in large parameter spaces.

Finally, a convenient feature of SIS clumps is that the mass only affects the Einstein radius  $b$ , and the cross section scales with  $\pi b^2$ . Thus, the scaled cross section  $\hat{\sigma} =$



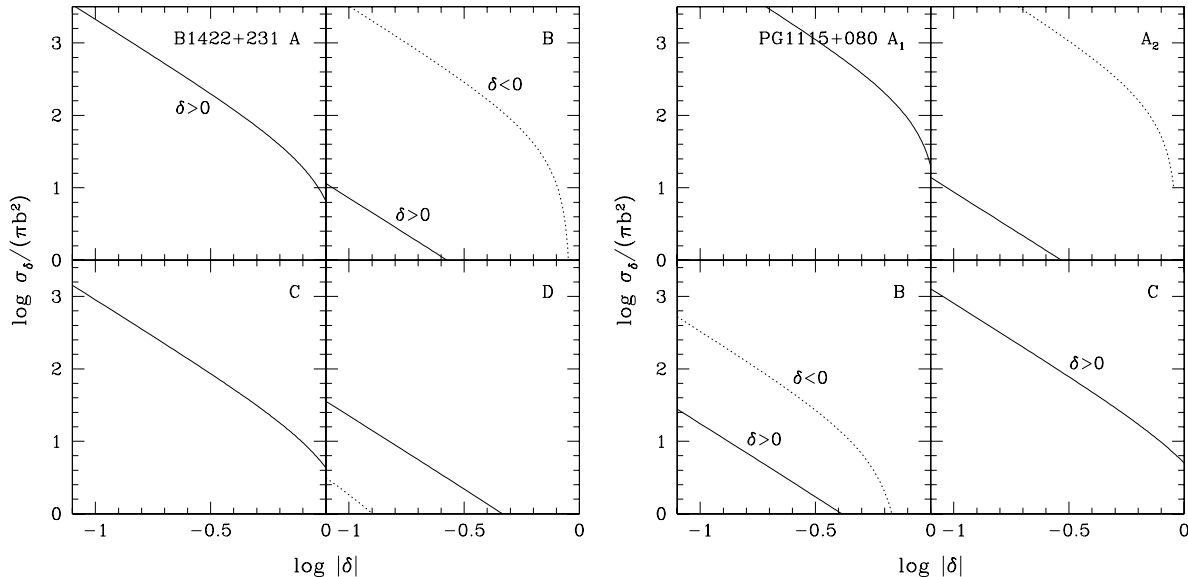


FIG. 9.— Estimates of the cross sections for magnification perturbations stronger than  $\delta$ . Solid curves are for  $\delta > 0$  and dotted curves are for  $\delta < 0$ . The clumps are assumed to lie in the lens galaxy ( $\beta = 0$ ). (Left) B1422+231. (Right) PG 1115+080.

$\sigma/(\pi b^2)$  is independent of clump mass, so we may write

$$\tau(\delta; \kappa, \gamma) = \pi \int_0^{z_s} dz D(z)^2 \frac{dD}{dz} \hat{\sigma}(\delta; \kappa, \gamma, \beta) \int dM \frac{dn}{dM} b^2. \quad (46)$$

The inner integral is just an integral over the mass function weighted by  $b^2$ . For SIS clumps,  $b \propto \sigma^2 \propto M^{2/3}$  (see eq. 2), so for mass functions steeper than  $dn/dM \propto M^{-4/3}$  the optical depth will be dominated by low-mass clumps.

## 5. CONCLUSIONS

In the context of substructure lensing, the general problem of a mass clump anywhere along the line of sight to a strong lens can be mapped onto an equivalent problem of a clump in a simple convergence and shear field; thus, the theory can easily accommodate clumps at arbitrary redshifts. If a clump can be approximated as an SIS, the clump plus external field problem is analytically tractable, yielding simple formulas for the cross sections relevant for substructure lensing. Both of these results will make it possible to explore substructure lensing effects in large parameter spaces quickly and easily.

The analytic results already reveal two interesting features of substructure lensing. First, the sign of the perturbation depends on the parity of the original image. SIS clumps always make positive-parity images brighter, and they usually make negative-parity images fainter. There is some probability that SIS clumps can make negative-parity images brighter, but it is usually much smaller than the probability of dimming, except for clumps far in redshift from the lens galaxy. The qualitative difference between positive-parity and negative-parity images has been remarked by Metcalf & Madau (2001) for perturbations by galactic subclumps, and studied in detail by Schechter & Wambsganss (2002; also Witt, Mao & Schechter 1995) for perturbations by stars. The effect is qualitatively similar for the two types of perturbers, although it appears to be more dramatic for stars. It is a distinctive feature

of substructure lensing (whether by stars or by larger, extended clumps) that will be useful for distinguishing the phenomenon from other systematic effects in lens flux ratios.

The second qualitative result is that a clump need not reside in the halo of the lens galaxy in order to have a significant lensing effect. Lensing is sensitive to clumps anywhere along the line of sight — not uniformly, but with a redshift dependence that I have quantified. The sensitivity function peaks at the lens redshift, but it has a width of several tenths in redshift and tails that extend to  $z = 0$  and to the source redshift. If CDM is right, isolated small halos may be much less abundant (per unit volume) than clumps within galaxy halos, but they are viable over such a large volume that they may still be relevant for substructure lensing. If WDM is right and galaxies are relatively smooth, isolated clumps could be the dominant cause of substructure lensing. Using predicted clump populations to evaluate the relative importance of isolated and embedded clumps is the subject of a work in progress (J. Chen et al., in preparation). This issue may ultimately affect how substructure lensing is interpreted, and how strongly it supports CDM and rules out WDM.

I would like to thank Andrey Kravtsov, Jackie Chen, and Daniel Holz for interesting discussions that stimulated this project. In particular, Andrey Kravtsov and Daniel Holz independently suggested that it might be worthwhile to consider isolated clumps. This work was supported by NASA through Hubble Fellowship grant HST-HF-01141.01-A from the Space Telescope Science Institute, which is operated by the Association of Universities for Research in Astronomy, Inc., under NASA contract NAS5-26555.

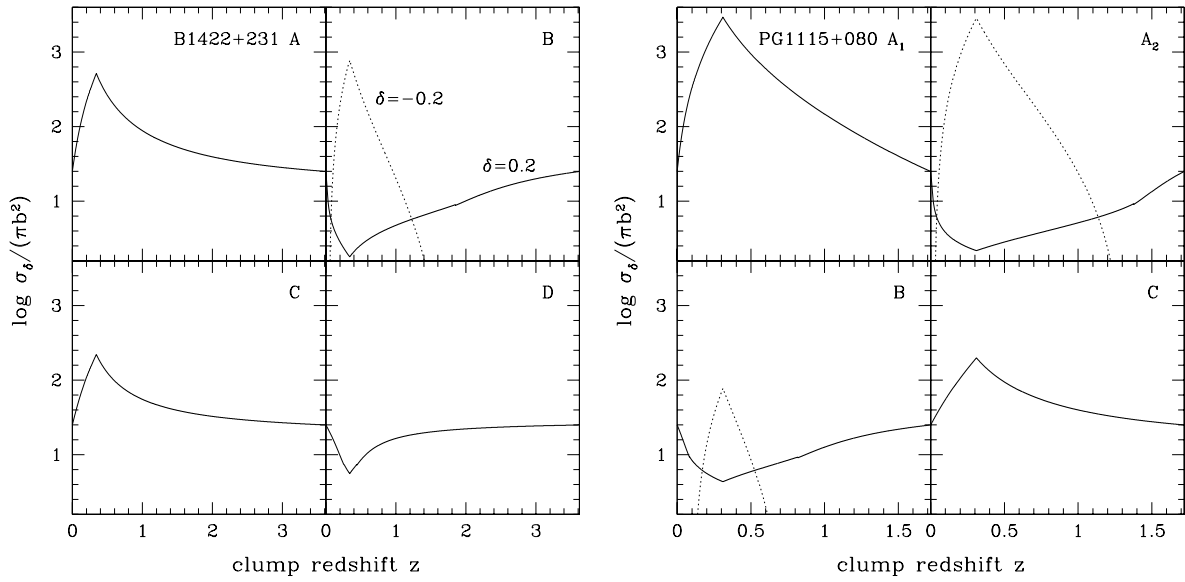


FIG. 10.— Estimates of the cross sections as a function of the clump redshift. Solid curves are for  $\delta = 0.2$  and dotted curves are for  $\delta = -0.2$ . Note that the area is given in units of the Einstein radius  $b$ , so effectively it is the Einstein radius (not the clump mass) that is held fixed as the redshift changes. The cosmology is  $\Omega_M = 0.3$  and  $\Omega_\Lambda = 0.7$ . (Left) B1422+231. (Right) PG 1115+080.

## REFERENCES

- Benson, A. J., Frenk, C. S., Lacey, C. G., Baugh, C. M., & Cole, S. 2002, *MNRAS*, 333, 177
- Bode, P., Ostriker, J. P., & Turok, N. 2001, *ApJ*, 556, 93
- Bradač, M., Schneider, P., Steinmetz, M., Lombardi, M., King, L. J., & Porcas, R. 2002, *A&A*, 388, 373
- Bullock, J. S., Kravtsov, A. V., & Weinberg, D. H. 2000, *ApJ*, 539, 517
- Chiba, M. 2002, *ApJ*, 565, 17
- Colin, P., Avila-Reese, V., & Valenzuela, O. 2000, *ApJ*, 542, 622
- Dalal, N., & Kochanek, C. S. 2002a, *ApJ*, 572, 25
- Dalal, N., & Kochanek, C. S. 2002b, preprint (astro-ph/0202290)
- Evans, N. W., & Wilkinson, M. I. 1998, *MNRAS*, 296, 800
- Fabbiano, G. 1989, *ARA&A*, 27, 87
- Finch, T., Carlivati, L. P., Winn, J. N., & Schechter, P. L. 2002, *ApJ*, 577, 51
- Hogg, D. W., & Blandford, R. D. 1994, *MNRAS*, 268, 889
- Impey, C. D., et al. 1998, *ApJ*, 509, 551
- Kassiola, A., & Kovner, I. 1993, *ApJ*, 417, 450
- Keeton, C. R., Kochanek, C. S., & Seljak, U. 1997, *ApJ*, 482, 604
- Keeton, C. R. 2001a, preprint (astro-ph/0102340)
- Keeton, C. R. 2001b, preprint (astro-ph/0111595)
- Keeton, C. R. 2002, preprint (astro-ph/0206243)
- Klypin, A., Kravtsov, A. V., Valenzuela, O., & Prada, F. 1999, *ApJ*, 522, 82
- Knebe, A., Devriendt, J. E. G., Mahmood, A., & Silk, J. 2002, *MNRAS*, 329, 813
- Kochanek, C. S. 1993, *ApJ*, 419, 12
- Kochanek, C. S. 1996, *ApJ*, 466, 638
- Kormann, R., Schneider, P., & Bartelmann, M. 1994, *A&A*, 286, 357
- Kundić, T., Cohen, J. G., Blandford, R. D., & Lubin, L. M. 1997a, *AJ*, 114, 507
- Kundić, T., Hogg, D. W., Blandford, R. D., Cohen, J. G., Lubin, L. M., & Larkin, J. E. 1997b, *AJ*, 114, 2276
- Lawrence, C. R., Elston, R., Januzzi, B. T., & Turner, E. L. 1995, *AJ*, 110, 2570
- Mao, S., & Schneider, P. 1998, *MNRAS*, 295, 587
- Maoz, D., & Rix, H.-W. 1993, *ApJ*, 416, 425
- Metcalf, R. B., & Madau, P. 2001, *ApJ*, 563, 9
- Metcalf, R. B., & Zhao, H. 2002, *ApJ*, 567, L5
- Moore, B., Ghigna, S., Governato, F., Lake, G., Quinn, T., Stadel, J., & Tozzi, P. 1999, *ApJ*, 524, L19
- Navarro, J. S., Frenk, C. S., & White, S. D. M. 1996, *ApJ*, 462, 563
- Patnaik, A. R., Browne, I. W. A., Walsh, D., Chaffee, F. H., & Foltz, C. B. 1992, *MNRAS*, 259, 1P
- Rix, H.-W., de Zeeuw, P. T., Carollo, C. M., Cretton, N., & van der Marel, R. P. 1997, *ApJ*, 488, 702
- Rusin, D., & Ma, C.-P. 2001, *ApJ*, 549, L33
- Schechter, P. L., & Wambsganss, J. 2002, preprint (astro-ph/0202425)
- Schneider, P., Ehlers, J., & Falco, E. E. 1992, *Gravitational Lenses* (New York: Springer)
- Somerville, R. S. 2002, *ApJ*, 572, L23
- Spergel, D. N., & Steinhardt, P. J. 2000, *Phys Rev Lett*, 84, 3760
- Tonry, J. L. 1998, *AJ*, 115, 1
- Tonry, J. L., & Kochanek, C. S. 1999, *AJ*, 117, 2034
- Treu, T., & Koopmans, L. V. E. 2002, *ApJ*, 575, 87
- Weymann, R. J., Latham, D., Angel, F. R. P., Green, R. F., Liebert, J. W., Turnshek, D. A., Turnshek, D. E., & Tyson, J. A. 1980, *Nature*, 285, 641
- Witt, H. J., Mao, S., & Schechter, P. L. 1995, *ApJ*, 443, 18